



Iron trifluoride synthesized via evaporation method and its application to rechargeable lithium batteries

Seung-Taek Myung^{a,b,*}, Shuhei Sakurada^b, Hitoshi Yashiro^b, Yang-Kook Sun^{c,**}

^a Department of Nano Engineering, Sejong University, 98 Gunja-dong, Gwangjin-gu, Seoul 143-747, Republic of Korea

^b Department of Chemistry and Bioengineering, Iwate University, 4-3-5 Ueda, Morioka, Iwate 020-8551, Japan

^c Department of WCU Energy Engineering, Hanyang University, Seoul 133-791, Republic of Korea

HIGHLIGHTS

- ▶ FeF₃ is readily synthesized via a direct reaction of Fe₂O₃ and HF.
- ▶ The resulting β-FeF₃·3H₂O transforms to FeF₃ at 400 °C in an Ar atmosphere.
- ▶ The FeF₃ delivers a high capacity of 224 mAh g⁻¹ with good capacity retention.
- ▶ This results from the maintenance of the crystal structure by topotactic reaction.

ARTICLE INFO

Article history:

Received 26 June 2012

Received in revised form

9 September 2012

Accepted 10 September 2012

Available online 17 September 2012

Keywords:

Evaporation synthesis

Iron trifluoride

Intercalation

Conversion

Lithium

Battery

ABSTRACT

Facile synthesis of rhombohedral type FeF₃ introduced via two consecutive steps is introduced: i) acidic treatment of Fe₂O₃ followed by thermal evaporation at 80 °C resulting in hydrated β-FeF₃·3H₂O and ii) a simple thermal decomposition of the as-received β-FeF₃·3H₂O at 400 °C under an Ar atmosphere. A Rietveld refinement of x-ray diffraction data for the as-synthesized FeF₃ indicates the formation of a highly crystalline FeF₃ structure with a $R\bar{3}c$ space group. To overcome the high ionicity and improve the diffusivity, FeF₃ is ball-milled with the aid of carbon (acetylene black). The electrochemical performance of nanosized FeF₃ is not favored in voltage range of 1.5–4.5 V because the repetitive intercalation–conversion reaction accelerates the structural disruption within a few cycles, although a high capacity (518 mAh (g-fluoride)⁻¹ at 20 mA g⁻¹) is observed, assisted by the three-electron redox of Fe^{3+/0}. Raising the lower cut-off voltage to 2 V, which allows only intercalation reaction, the FeF₃ delivers a high capacity of 224 mAh g⁻¹ with significantly improved capacity retention (71% at 100th cycle).

© 2012 Elsevier B.V. All rights reserved.

1. Introduction

Recently, metal fluorides and metal fluoride nanocomposites have been of great interest for potential use as next-generation high capacity electrode materials [1–18]. These materials show a different type of electrochemical reaction, compared to typical lithiated transition metal oxides (LiMO₂, M = Co, Ni, and Mn) that are in commercially available rechargeable lithium batteries. Instead of reversible insertion and extraction of Li ions, the metal

fluorides offer a full reduction to the metallic state and reconversion to the original host structure, i.e., metal fluorides, attaining multi-electron transfers of up to 3e⁻ per transition metal. This chemistry gives rise to higher capacity than the conventional lithiated transition metal oxides, which allows no more than 1 mol of Li ion per formula unit during an insertion or extraction reaction. In addition, the unusually high ionicity of metal fluorides provides a high operation voltage during the electrochemical reaction with lithium.

Tracing back to its introduction in the 1970s, HgF₂ showed a capacity based on the conversion reaction in a primary lithium cell [19]. Among metal fluorides [17], FeF₃ exhibited a relatively high operation voltage during Li⁺ insertion such that it is expected to be used as a positive electrode material. As iron is the most abundant element in the earth, utilization of iron-based material is very attractive in terms of material cost and non-toxicity. Owing to

* Corresponding author. Department of Nano Engineering, Sejong University, 98 Gunja-dong, Gwangjin-gu, Seoul 143-747, Republic of Korea. Tel./fax: +82 2 3408 3454.

** Corresponding author. Tel.: +82 2 2220 0524; fax: +82 2 2282 7329.

E-mail addresses: smyung@sejong.ac.kr (S.-T. Myung), yksun@hanyang.ac.kr (Y.-K. Sun).

its insulating character, FeF_3 , however, always suffers from poor kinetics. For example, Arai et al. [1] reported that FeF_3 could result in over 50% utilization and a limited degree of reversibility. Significant improvement was first achieved by Amatucci et al. [2,3] with the formation of a carbon-nanocrystalline FeF_3 composite, delivering a discharge capacity of 660 mAh g^{-1} at 70°C with the aid of a conversion reaction in the voltage range of 1.5–4.5 V. Further modification with carbonaceous materials endowed greater improvement in the capacity, reversibility, and rate capability [7,10,16]. Low heat generation originating from the stable structure also confirmed better thermal stability in contrast to LiMO_2 ($\text{M} = \text{Co}, \text{Ni}, \text{and Mn}$) materials [13]. The electrochemical reaction of FeF_3 is associated with two kinds of processes, intercalation and conversion, as proposed by Badway et al. [2,3] and Li et al. [4]. For intercalation, Li ions are inserted into the FeF_3 framework via a two-phase region to form $\text{Li}_{0.5}\text{FeF}_3$ and then via a one-phase region, forming LiFeF_3 , which appears in the 2.5–4.5 V range. Then, the formed LiFeF_3 is subject to decomposition to LiF and Fe metal after reacting with 2 moles of Li, which is observed in the 1.5–2.5 V conversion reaction.

Nonetheless, only a few papers have dealt with the synthesis of FeF_3 [4,7,12]. Cases with higher capacities and better rate capabilities compared to the commercialized FeF_3 were observed [1–5,8,9,13,16–18]. Crouse [20] reported the synthesis of $\text{FeF}_3 \cdot 3\text{H}_2\text{O}$ by dissolving iron powders in an HF and HNO_3 mixture. Here, facile synthesis of FeF_3 and the resulting electrochemical properties are reported.

2. Experimental

2.1. Synthesis of FeF_3

Fe_2O_3 (Wako) was immersed in an HF solution (46 wt. %, Wako) in a Teflon beaker (200 ml) and magnetically stirred at 25°C for 24 h in air. Then, the reaction temperature was raised to 80°C to slowly remove the solution to yield a light yellow powder. The product was calcined in the temperature range of 200–400 $^\circ\text{C}$ for 5 h in an Ar atmosphere to prevent any reactions with oxygen. The produced pale green FeF_3 and acetylene black (weight ratio of calcined product:acetylene black = 85:15) were milled in a zirconia jar with zirconia balls using a planetary ball mill at 600 r.p.m. for 1 h in an N_2 atmosphere to prevent any reaction with oxygen and moisture during milling.

2.2. Structural properties

The as-received powders were subjected to thermal gravimetric analysis (TGA, loaded sample amount: 10 mg, DTG-60, SHIMADZU, Japan). The crystalline phase of the products was characterized by powder x-ray diffraction (XRD, Rint-2000, Rigaku) analysis using $\text{Cu-K}\alpha$ radiation. The XRD data were obtained at $2\theta = 10\text{--}80^\circ$, with a step size of 0.03° and a count time of 5 s. The collected intensity data from the XRD were analyzed by the Rietveld refinement program Fullprof 2002 [21]. The particle morphologies of the produced powders were observed using scanning electron microscopy (SEM, JXA-8100, JEOL) and transmission electron microscopy (H-800, Hitachi).

2.3. Electrochemical properties

Electrodes were fabricated using a mixture of milled FeF_3 -acetylene black composite (95:5 wt. %) and polyvinylidene fluoride (5 wt. %) in *N*-methylpyrrolidinon, where the ratio of FeF_3 :acetylene black:binder was 80.75:14.25:5. The slurry was spread onto Al foil and dried in an oven at 85°C . The electrode was subsequently dried

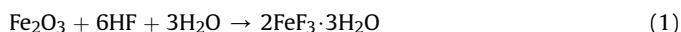
overnight at 120°C under vacuum and then roll-pressed prior to use. Electrochemical properties were measured using R2032 coin-type cells with a Li metal negative electrode. The electrolyte solution was 1 M LiPF_6 in a 1:1 volume mixture of ethylene carbonate and diethyl carbonate. The cells were assembled in an argon-filled glove box.

2.4. Electrochemically de-lithiated electrodes

Electrochemically de-lithiated/lithiated electrodes were examined using XRD to understand the structure in the compounds. Those electrodes were rinsed with salt-free diethyl carbonate to remove the residual salt, followed by drying at 80°C in the glove box. The electrodes were wrapped with a Mylar film (Chemplex™) for the XRD measurement in which Al foil was used as an internal standard.

3. Results and discussion

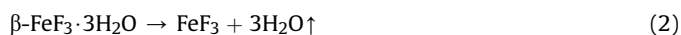
XRD pattern of the as-precipitated powders are shown in Fig. 1a, which was consistent with the diffraction pattern of $\beta\text{-FeF}_3 \cdot 3\text{H}_2\text{O}$ [22] (space group $P4/m$, $a=7.8378(1) \text{ \AA}$ and $c=3.8793(2) \text{ \AA}$ calculated by a least square method). There are no impurities derived from Fe–O or other Fe–F compounds in the XRD pattern. Formation of $\alpha\text{-FeF}_3 \cdot 3\text{H}_2\text{O}$ is not possible under the present experimental conditions because the α -form is stable and maintains its structure when it is formed below 50°C [23]. Also, the α -form tends to convert to the β -form within days even at room temperature. Earlier work by Crouse [20] indicated that metallic Fe powders reacting with HF and HNO_3 could be used to form $\beta\text{-FeF}_3 \cdot 3\text{H}_2\text{O}$. In this experiment, Fe_2O_3 was selected as a starting material since the oxide is stable in air and also readily soluble when the solution pH is below 2. Thus, the following reaction is likely to occur to give precipitates after evaporation of the solution at 80°C :



The particle morphology of the starting Fe_2O_3 (Fig. 1b) was no longer observed in the products after the above reaction (Fig. 1c).

The as-synthesized $\beta\text{-FeF}_3 \cdot 3\text{H}_2\text{O}$ was analyzed by TGA to determine the optimum heat-treatment temperature (Fig. 2). The measurement was carried out in the temperature range of 50–800 $^\circ\text{C}$ in an Ar atmosphere. There was no apparent change in weight from room temperature up to 100 $^\circ\text{C}$. A simple one-step weight loss was observed in the temperature range of 115–370 $^\circ\text{C}$, showing 33.2 wt. % of weight loss. In this temperature range, crystal water is removed from the $\beta\text{-FeF}_3 \cdot 3\text{H}_2\text{O}$ compound to form dehydrated FeF_3 . A possible factor for the slightly higher value comparing with the theoretical one (32.4 wt. %) would be due to the evaporation of the adhered water during sample treatment. Then, a mild variation in weight is observed up to 780 $^\circ\text{C}$, which results from the partial evaporation of F from the dehydrated compound. This analysis suggests that dehydration at 400 $^\circ\text{C}$ is appropriate to form the water-free FeF_3 compound.

Thus, the precipitated $\beta\text{-FeF}_3 \cdot 3\text{H}_2\text{O}$ was fired for 5 h at 400 $^\circ\text{C}$ in an Ar atmosphere to avoid reaction with oxygen in the tube furnace. After heat-treatment at 400 $^\circ\text{C}$, where the evaporation of the crystal water completed (Fig. 2), the $\beta\text{-FeF}_3 \cdot 3\text{H}_2\text{O}$ is transformed to a phase-pure high crystalline FeF_3 (Fig. 3a) by the following reaction:



To further investigate the crystal structure of the as-synthesized FeF_3 , Rietveld refinement of the XRD pattern was carried out based

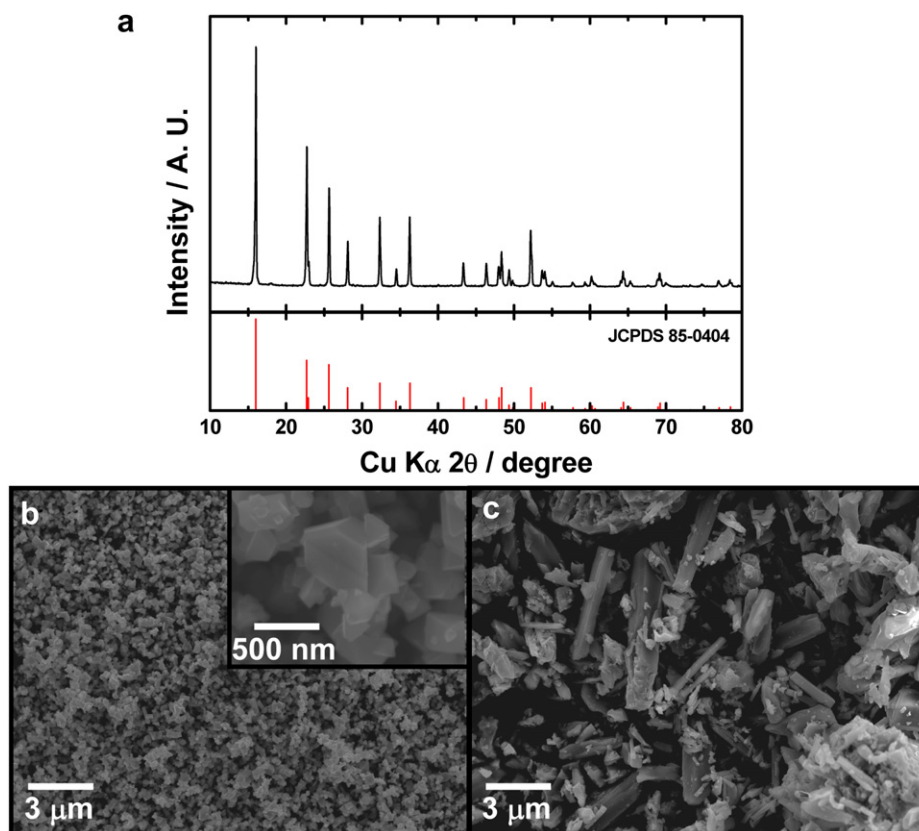


Fig. 1. (a) XRD pattern of the as-synthesized $\beta\text{-FeF}_3 \cdot 3\text{H}_2\text{O}$; SEM image starting (b) Fe_2O_3 and (c) as-synthesized $\beta\text{-FeF}_3 \cdot 3\text{H}_2\text{O}$.

on $R\bar{3}c$ space group, and the resulting data are shown in Fig. 3a and Table 1. Chemical composition was fixed to FeF_3 due to refinement error when F content varied. The observed pattern is in good agreement with the calculated one, as the reliable factors are sufficiently small (R_{wp} : 9.11%, R_B : 2.74%). Further, there is no trace of a $\beta\text{-FeF}_3 \cdot 3\text{H}_2\text{O}$ -related compound in the refined XRD pattern, indicating that the contained crystal water no longer exists in the product. Calculated lattice parameters are $a = 5.2049(2)$ Å and $c = 13.3336(5)$ Å, of which the values of which are close to the reported values [12,16]. The Fe–F length in FeF_3 is calculated to be 1.9212(6) Å, which is in accordance with earlier reports [12,24]. In consideration of the ionic radius of Fe^{3+} (high spin, 0.645 Å: coordination number, 6 [25]) and F^- (1.285 Å: coordination number, 2 [25]), the observed value coincides with the estimated value. The irregular $\beta\text{-FeF}_3 \cdot 3\text{H}_2\text{O}$ particles (Fig. 1c) were altered to rectangular or square-shaped particles (Fig. 3b), and the observed particle size ranged from 1 to 3 μm after the heat treatment. An XPS investigation was carried out to evaluate the chemical state of Fe for the as-prepared FeF_3 with comparison to the simulated spectrum of $\text{Fe}^{\text{III}}\text{F}$ (Fig. 3c) [26]. Trivalent Fe_2O_3 usually exhibits its binding energy at 710.9 eV [26]. The strong ionic character of the FeF_3 , however, causes a shift in the resulting binding energy, approximately 3.5 eV greater than that of the oxide. The XPS spectrum of the as-synthesized FeF_3 is consistent with the simulated $\text{Fe}^{\text{III}}\text{F}_3$. The above results indicate that FeF_3 can be readily synthesized through the dehydration of $\beta\text{-FeF}_3 \cdot 3\text{H}_2\text{O}$, which was prepared via the direct evaporation of a Fe_2O_3 -dissolved HF solution in an inert atmosphere.

Meanwhile, the wide energy gap between conduction and valence bands of FeF_3 , approximately 5.96 eV [12], resulting in poor electronic conductivity, is likely to restrict the application of FeF_3 as an electrode material for rechargeable lithium batteries. The

electronic limitations can be overcome by processing with materials such as carbon-coating, mechano-milling and so on. Since graphitization of carbon coating layer is available when the temperature is greater than 700 °C [27,28], the coating would not be readily applicable for the present material due to the evaporation of F during heating at high temperature. A reduction in particle size, which improves Li^+ diffusion by shortening the diffusion path, would be better to enhance the restricted poor electronic conductivity. Thus, as-synthesized FeF_3 was ball-milled with acetylene black (AB) at a weight ratio of 85:15 in a N_2 atmosphere to prevent

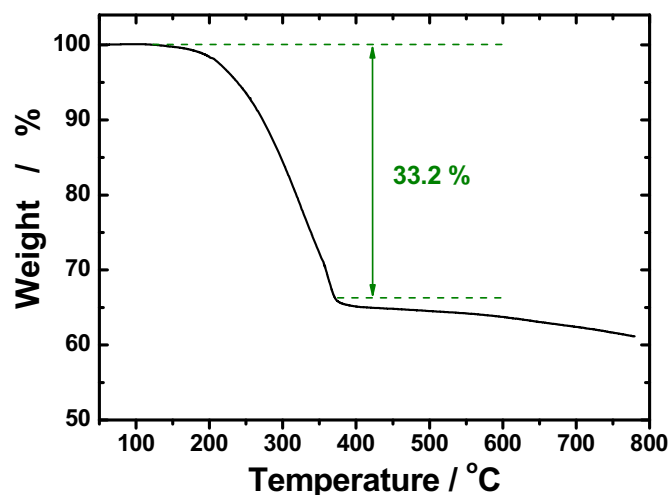


Fig. 2. Thermogravimetric curve of the as-synthesized $\beta\text{-FeF}_3 \cdot 3\text{H}_2\text{O}$. The measurement was made in an Ar atmosphere.

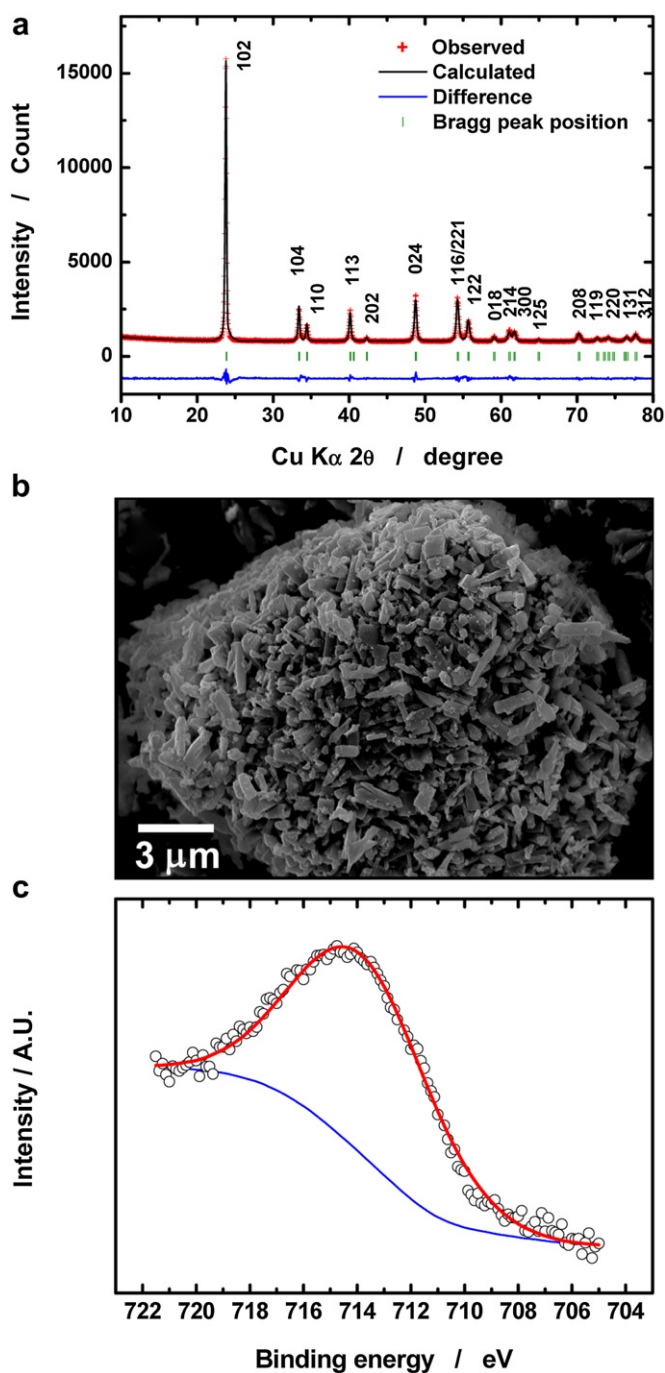


Fig. 3. (a) Rietveld refinement of XRD data of the as-synthesized FeF_3 and (b) the resulting SEM image, and (c) XPS spectrum of FeF_3 .

reaction with air and oxidation induced from heat generated during the milling. The added AB is likely to improve electronic conductivity and also provides a reductive environment during ball-milling. The corresponding XRD pattern of the ball-milled product was compared with that of the as-synthesized FeF_3 (Fig. 4a and b). There is no difference in the lattice parameter after the milling, although apparent peak broadening is observed (Fig. 4b), indicating that the induced peak broadening merely originated from the reduction in crystallite size. Using the Williamson–Hall equation, the calculated average crystallite size was found to be approximately 30 nm. The TEM image confirms that the as-synthesized FeF_3 particles are obviously reduced and

Table 1
Structural parameters obtained from Rietveld refinement results of XRD data for $\beta\text{-FeF}_3 \cdot 3\text{H}_2\text{O}$ heated at 400 °C for 5 h in an Ar atmosphere.

Formula crystal system space group		FeF_3 Rhombohedral $R\bar{3}c$				
Atom	Site	x	y	z	g	$B/\text{\AA}^2$
Fe	6b	0	0	0	1	0.8
F	18e	0.585(5)	0	0.25	1	0.7
$a/\text{\AA}$		5.2049(2)				
$c/\text{\AA}$		13.3336(5)				
Fe–F/ \AA		1.9212(6)				
$R_{\text{wp}}/\%$		9.11				
$R_{\text{B}}/\%$		2.74				
$(R_{\text{wp}}/R_{\text{exp}})^2$		1.24				

modified by the AB carbon (Fig. 4c) (hereafter referred to as C/ FeF_3), as carbon was detected in the XRD pattern (Fig. 4b).

The electrochemical performance of the as-prepared FeF_3 and C/ FeF_3 electrode were investigated in the voltage range of 1.5–4.5 V by applying 20 mA g^{-1} at 25 °C (Fig. 5a). Due to the absence of lithium in the compound, discharge (reduction) was first conducted from an open-circuit voltage. The as-prepared FeF_3 without ball-milling delivers lower capacity and lower operation voltage. Meanwhile, a short but flat voltage is observed at 3.3 V ($\sim 90 \text{ mAh g}^{-1}$), after which a monotonous voltage decrease is found up to 2.9 V ($\sim 135 \text{ mAh (g-fluoride)}^{-1}$). Then, the voltage abruptly drops to 1.75 V. After that, two long voltage plateaus appeared, delivering a capacity of about 261 mAh g^{-1} ; the former plateau shows a capacity approximately 146 mAh g^{-1} and the latter

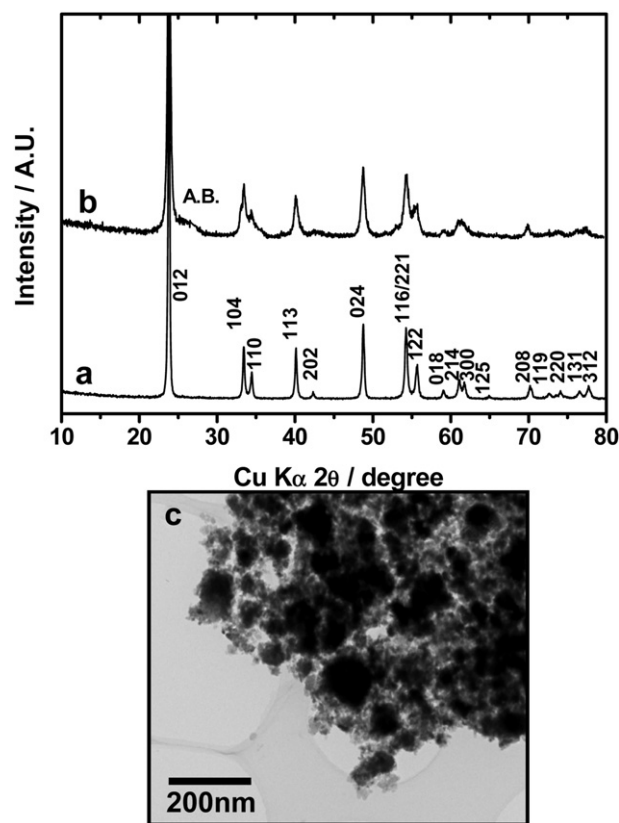


Fig. 4. XRD patterns of (a) as-synthesized FeF_3 and (b) ball-milled FeF_3 with acetylene black; (c) corresponding TEM bright-field image of the ball-milled FeF_3 with acetylene black.

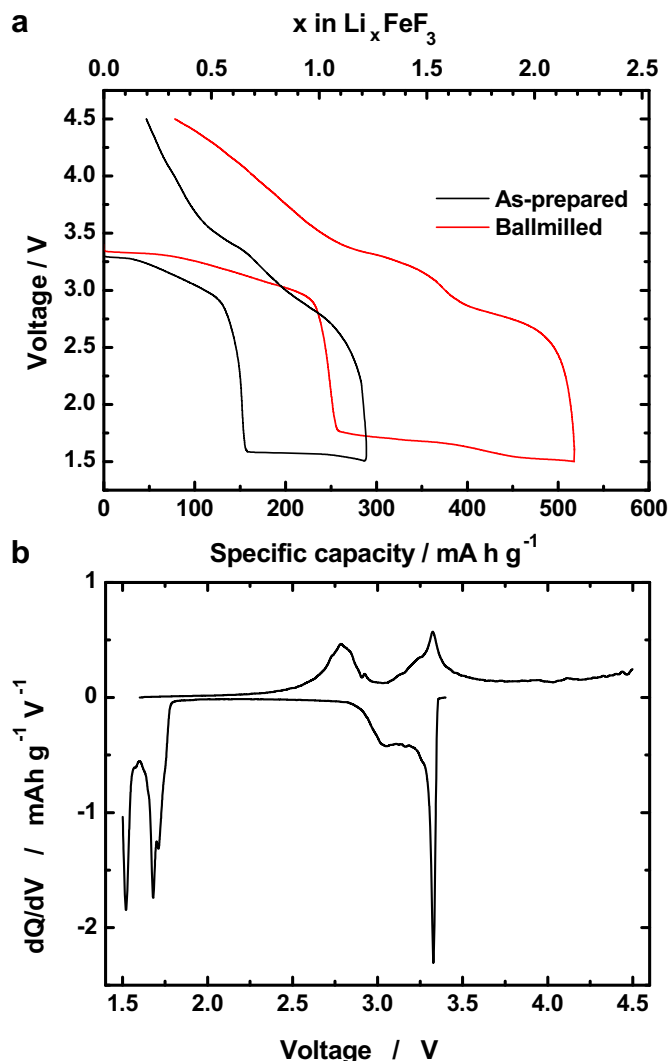


Fig. 5. (a) Comparison of first discharge and charge curve of as-prepared FeF_3 and ballmilled C/FeF_3 electrode and (b) corresponding differentiated curves of C/FeF_3 electrode.

corresponds to 115 mAh g^{-1} . This feature is also confirmed in its derivative form, shown in Fig. 5b. The first two plateaus are observed at 3.3 V and 2.9 V; the flat plateau at 2.9 V is ascribed to the two-phase reaction, and the slow slope at 2.9 V is due to a one-phase reaction. They are slightly higher than those observed for commercial FeF_3 and the resulting capacity to 2 V as well [1–5,8,9,13,16–18]. The second two plateaus are located at 1.75 V and 1.55 V. It is considered that the difference in the operation voltage comparing to the commercial FeF_3 would be ascribed to the crystallinity. Since commercial FeF_3 is practically prepared as follows: $\text{FeCl}_3 + 3\text{HF} \rightarrow 2\text{FeF}_3 + 3\text{HCl}$ without heat-treatment, the resulting crystallinity is considered to be lower than the present material that is fired at 400°C . Although the produced FeF_3 was ballmilled (Fig. 4b), the full-width of half maximum of diffraction peaks is still smaller than those of ballmilled commercial FeF_3 [1–5,8,9,13,16–18], providing better structural integrity during Li^+ insertion.

Upon charging, a reversible reaction occurs, although the voltage gap between charge and discharge was greater presumably because of the poor electronic conductivity. The delivered charge capacity is about 440 mAh g^{-1} in the voltage range of 1.5–4.5 V (Fig. 5a). The charge curve is composed of three plateaus. The first voltage plateau is observed at 2.8 V and the second plateau

appears at 3.3 V, after which the voltage increases monotonously to 4.5 V (the third plateau) in Fig. 5a and b. A capacity of approximately 78 mAh g^{-1} , which corresponds to 0.32 Li, is not recovered. The difference between the charge and discharge voltage is ascribable to the highly ionic character of the metal-fluoride bond in the crystal lattice, which perturbs Li ion diffusion.

To understand the discharge–charge process, ex-situ XRD measurements were made at several points. After reaching the desired voltage, the electrodes were rinsed with a salt-free solvent (DMC) to remove residual lithium salt adhering to the surface of the electrodes, and they were then dried at 80°C in a glove box. As seen in Fig. 6a, there are two striking features after lithiation to $\text{Li}_{0.97}\text{FeF}_3$, compared with Li_0FeF_3 : i) the drastic decrease in the relative intensity of the (024) peak and ii) the manifest peak splits of the (104)/(110), (116/221)/(112), and (214)/(300) pairs. The only difference between Li_0FeF_3 and $\text{Li}_{0.97}\text{FeF}_3$ is that Li ions occupy the empty tunnels ([024] plane). The occupation of free sites by lithium ions is likely to affect the lattice environment neighboring the Li atoms, and this, in turn, would induce the peak splits. Variation in the lattice parameter after lithiation results in a considerable change in the lattice parameter, particularly the c-axis. Namely, Li^+ insertion into FeF_3 induces a tremendous variation in the c-axis of approximately 0.87 \AA (Fig. 7a), which is almost four-fold greater value than the c-axis variation of the other layered transition metal oxides [29–31]. Structural disintegration is also imaginable in view of the structural variation. Even conventional oxide electrode materials seem not to allow such an elongation of the c-axis. If this did happen, their structure would be readily transformed to other types of structures. It is speculated that the highly ionic character of the iron-fluoride bond is responsible for the tolerance of the original structure by forming a solid-solution between FeF_3 and LiFeF_3 , although the lattice varied significantly in the c-axis direction. The linear variation in the lattice parameters indicates a progressive Li^+ insertion reaction in this range, as suggested by Arai et al. [1] and

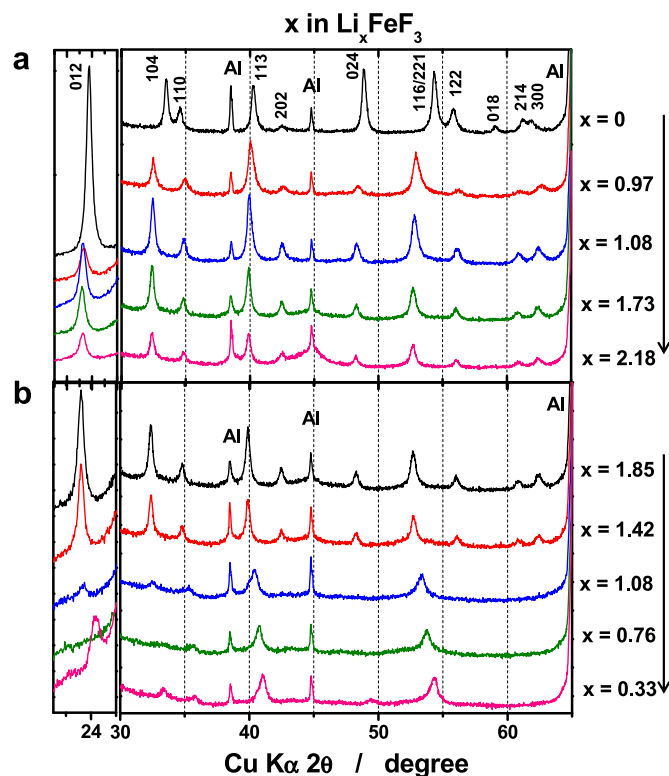


Fig. 6. Ex-situ XRD patterns of C/FeF_3 during the first (a) discharge and (b) charge.

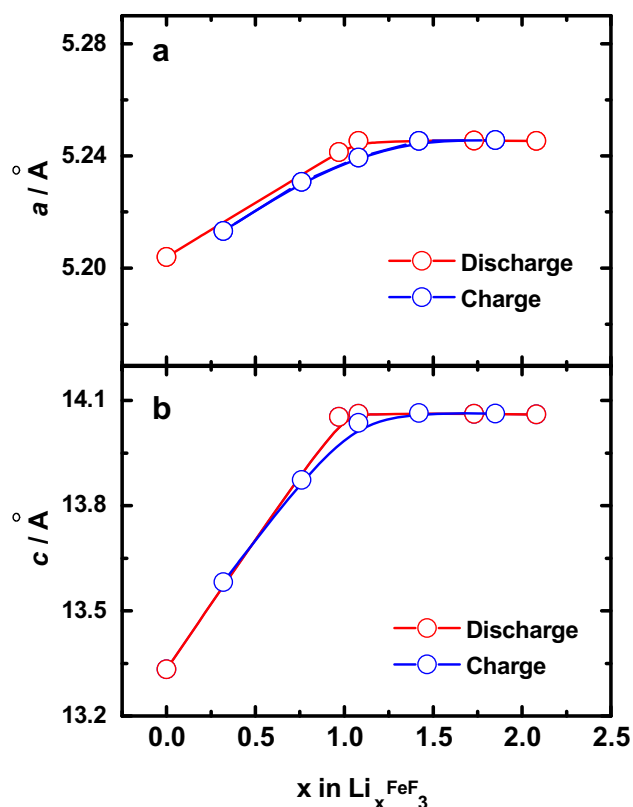


Fig. 7. Variation in lattice parameters of C/Li_xFeF₃ during the first discharge and charge; (a) *a*-axis and (b) *c*-axis.

Badway et al. [2], by the following reaction: $\text{Fe}^{\text{III}}\text{F}_3 + \text{Li}^+ + \text{e}^- \rightarrow \text{LiFe}^{\text{II}}\text{F}_3$. Thus, the XRD pattern would be that of the LiFeF_3 . Due to a lack of structural data, it is unfortunately not possible to compare the present lattice parameters of $\text{LiFe}^{\text{II}}\text{F}_3$ to those reported in the literature.

Structural evolution is not so pronounced by further lithiation from $\text{Li}_{0.97}\text{FeF}_3$, except for the growth of a (104) peak for $x = 1.08$ in Li_xFeF_3 . When $x = 1.73$ in Li_xFeF_3 (corresponding to a capacity of 415 mAh g^{-1} delivered), a small broad peak with Al at 45° (2θ) appears, compared with the XRD pattern of $\text{Li}_{1.08}\text{FeF}_3$. The peak broadens more in the range of $43\text{--}47^\circ$ (2θ) for $\text{Li}_{2.18}\text{FeF}_3$. The major XRD peaks of LiF and Fe^0 are located near 45° (2θ), and this may be attributed to the appearance of the broad hill in the range of $43\text{--}47^\circ$ (2θ) followed by the conversion reaction proposed by Badway et al. [4]: $\text{LiFe}^{\text{II}}\text{F}_3 + 2\text{Li}^+ + 2\text{e}^- \rightarrow 3\text{LiF} + \text{Fe}^0$. The presence of low crystallinity or nanocrystallites of the formed byproducts, such as LiF and Fe, may lead to broadening of the diffraction peak. One interesting feature is that excessive lithiation resulting in the lower voltage plateau did not result in notable structural variation in the XRD patterns (Fig. 6a). This phenomenon is further evidenced by the calculated lattice parameters of both the *a*- and *c*-axes that remained constant in this range (Fig. 7a and b).

There is no remarkable structural change during delithiation (oxidation), except for a decrease in the intensities of LiF and Fe reflections for $x=1.85$ and 1.42 in Li_xFeF_3 (Fig. 6b). In this range, the calculated lattice parameters are also kept constant as the same values are recognized in the same range during lithiation (Fig. 7a and b). This implies that the conversion reaction occurs reversibly. From the end point of the lower voltage plateau or the beginning point of the upper voltage plateau ($x = 1.08$ in Li_xFeF_3), the XRD pattern begins to slightly shift to a lower angle, and the resulting intensity becomes quite a bit lower; though the (113) and the (116)/(221) peaks were visible, broadening of these peaks more or less

progresses. The diffraction peaks are further shifted to a lower angle until $x=0.33$ in Li_xFeF_3 , implying ongoing deintercalation, where a gradual increase in the operation voltage was noted (Fig. 5a). A linear decrease in the lattice parameters also suggests oxidation of the iron. This is indicative of a progressive deintercalation reaction. Deintercalation, after undergoing the conversion reaction, however, does not seem to be favored because of the structural disintegration, resulting in the significantly lower relative intensity of the XRD patterns (Fig. 6b). The above XRD results confirm two reversible reactions: intercalation on the higher voltage plateau and conversion on the lower voltage plateau.

In order to confirm the continuous reversibility of both the intercalation and conversion reactions, charge–discharge tests were performed in the voltage range of $1.5\text{--}4.5 \text{ V}$ at 20 mA g^{-1} (Fig. 8a). After the first cycle, the resulting capacity greatly

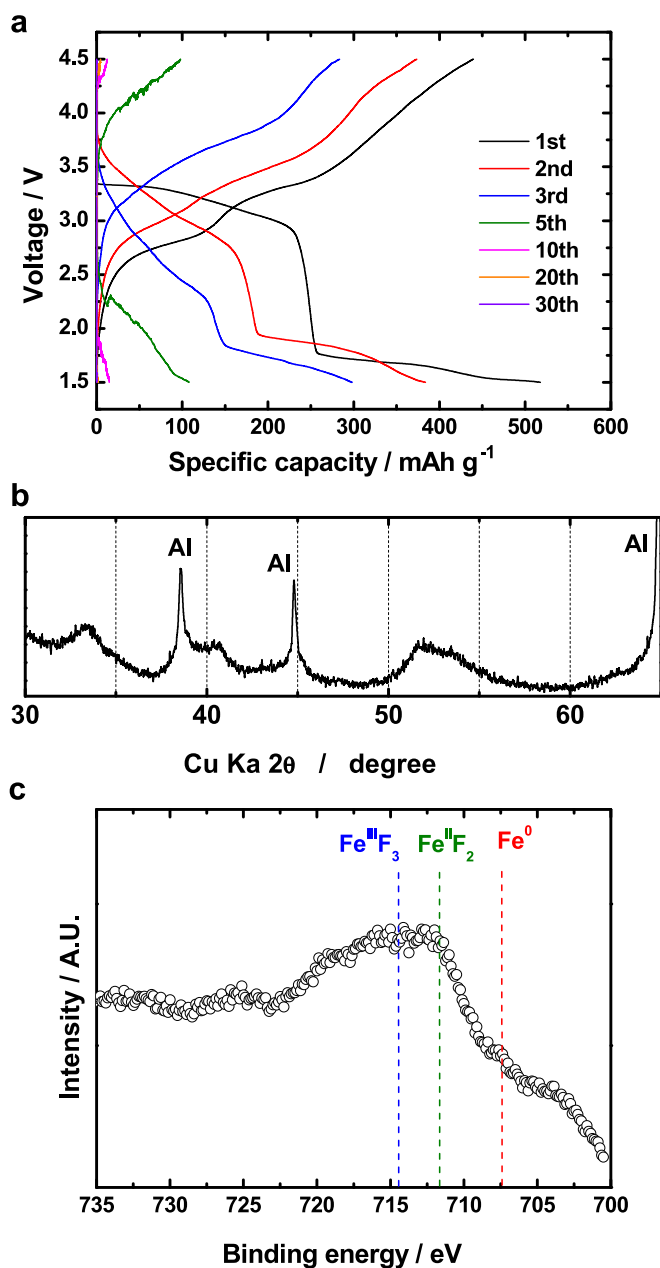


Fig. 8. (a) Continuous charge and discharge curves of C/FeF₃ in the voltage range of $1.5\text{--}4.5 \text{ V}$, (b) resulting XRD pattern, and (c) XPS spectrum of the C/FeF₃ electrode after 50 cycles.

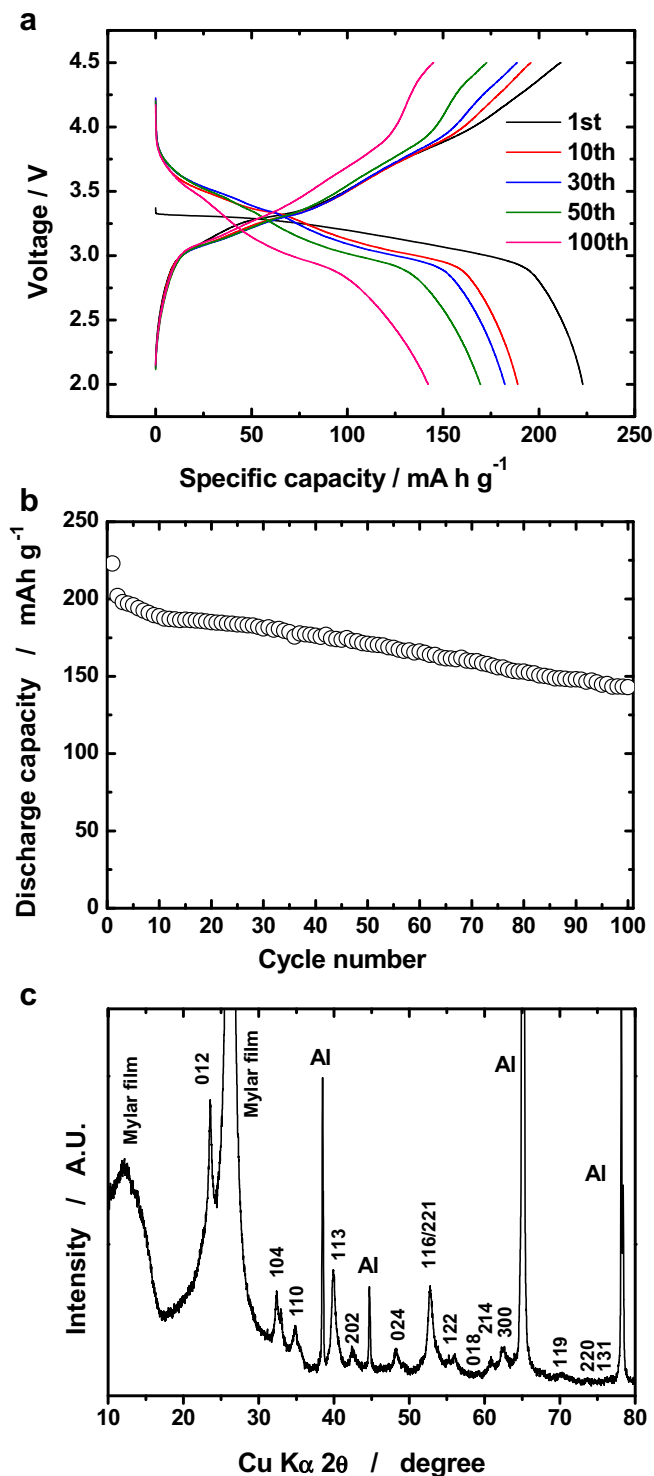


Fig. 9. (a) Continuous charge and discharge curves of C/FeF₃ in the voltage range of 2–4.5 V, (b) corresponding cyclability, and (c) XRD patterns of the C/FeF₃ electrode after 100 cycles. The high intensity in range of 10–30° in 2θ is due to reflection of the Mylar film used for the XRD measurement.

decreases, and the capacity associated with intercalation is not observed from the fifth cycle, after which the cell was no longer cyclable. The XRD pattern of the cycled C/FeF₃ electrode reveals that the original crystal structure could not be retained with cycling along with the repetitive intercalation and conversion reaction, thereby causing amorphization. In particular, the conversion

reaction always undergoes a phase transformation from divalent LiFe^{II}F₃ to Fe⁰ metal and *vice versa*. Both phases, however, have completely different structures, namely, LiFeF₃ (*R*3c) and Fe (*Im*3m). The phase transformation to each different phase would arouse tremendous stress in the crystal lattice during the repetitive conversion reaction, and the resulting structure would be randomized, exhibiting exceptionally broadened diffraction peaks (Fig. 8b). Furthermore, the remaining LiF, a byproduct resulting from the conversion reaction, would increase the electrode resistance due to its insulating property. XPS analysis was performed for the electrode of C/FeF₃ cycled in range of 1.5–4.5 V (Fig. 8c). As seen in the figure, the binding energies related with Fe⁰, Fe^{II}F, and Fe^{III}F are found due to the structural disruption induced by the consecutive conversion reaction. These complications are associated with the poor cycling performance in the voltage range of 1.5–4.5 V.

Thus, the lower cut-off voltage was raised to 2 V to prevent the conversion reaction. As seen from the continuous cycling curves (Fig. 9a), there are no marked changes in the charge-discharge profiles except for the first cycle. The delivered first discharge capacity is approximately 224 mAh g⁻¹, and the higher capacity is retained throughout the cycling test with capacity retention of 71% (143 mAh g⁻¹ at the 100th cycle) from the second cycle (Fig. 9b).

The XRD pattern of the cycled electrode also shows that the FeF₃ structure was not collapsed upon cycling in the voltage range of 2–4.5 V (Fig. 9c). Since a deteriorative conversion reaction did not take place in the voltage region, Li ions could diffuse through the empty channel of the FeF₃ structure, accompanied by progressive formation of a solid-solution between Fe^{III}F₃ and LiFe^{II}F₃. The empty channel is sufficiently large to accommodate or release Li ions from the structure, and in turn, this enabled retention of the structure along with the Fe^{2+/3+} redox. Apparently, the obtained capacity is comparable to other lithiated transition metal oxides [29–31] or phosphates [32,33]. Moreover, FeF₃ is known to have excellent thermal properties with low heat generation, as reported by Zhou et al. [13]. Recent work by Wang et al. [34] suggests superiority of conversion reaction in FeF₂, in contrast to FeF₃ exhibiting poor capacity driven by conversion reaction (Fig. 8a) presumably due to the formation of more amount of insulating LiF (3 mol, LiFe^{II}F₃ + 2Li⁺ + 2e⁻ → 3LiF + Fe) in the FeF₃ matrix compared to FeF₂ (2 mol, Fe^{II}F₂ + 2Li⁺ + 2e⁻ → Fe + 2LiF), because of the formation of a bicontinuous Fe network embedded in an insulating LiF matrix, which provides a pathway for local electron transport. Provided that the carbon coating method is established to improve the battery performance, like LiFePO₄, the present electrode material, FeF₃, would be worth revisiting as a potential cathode material for rechargeable lithium batteries.

4. Conclusion

FeF₃ is readily synthesized by the thermal decomposition of β-FeF₃·3H₂O, which is produced via the acidic treatment (below pH 2) of Fe₂O₃ at ambient temperature. Because of the existing strong ionicity, the as-synthesized FeF₃ is ball-milled in the presence of acetylene black to improve the poor electronic conductivity and thus shorten the diffusion path. Although a large capacity of 518 mAh g⁻¹, which is associated with the three-electron redox, is delivered during the first discharge, the consecutive cycling result is disappointing due to structure disintegration caused by the repetitive intercalation–conversion reaction between LiFeF₃ and Fe metal. The electrode performance of FeF₃ is drastically improved by maintaining the lower cut-off voltage at 2 V, yielding a simple topotactic reaction. The retained capacity reaches about 71% of the initial capacity (143 mAh g⁻¹) at the 100th cycle in the voltage range of 2–4.5 V. Since there are sufficient channels to accept the Li ion intercalation into the structure in the voltage range above 2 V,

the original structure is able to be maintained intact. Modification of the FeF_3 surface using conducting materials such as LiFePO_4 is necessary to improve the electrode performance for rechargeable lithium batteries.

Acknowledgment

This study was supported by a grant from the National Research Foundation of Korea funded by the Korean government (MEST) (NRF-2009-C1AAA001-0093307).

References

- [1] H. Arai, S. Okada, Y. Sakurai, J.-I. Yamaki, J. Power Sources 68 (1997) 716.
- [2] F. Badway, F. Cosandey, N. Pereira, G.G. Amatucci, J. Electrochem. Soc. 150 (2003) A1209.
- [3] F. Badway, F. Cosandey, N. Pereira, G.G. Amatucci, J. Electrochem. Soc. 150 (2003) A1318.
- [4] H. Li, G. Richter, J. Maier, Adv. Mater. 15 (2003) 736.
- [5] H. Li, P. Balaya, J. Maier, J. Electrochem. Soc. 151 (2004) A1878.
- [6] Y. Makimura, A. Rougier, L. Laffont, M. Womes, J.-C. Jumas, J.B. Leriche, J.-M. Tarascon, Electrochem. Commun. 8 (2006) 1769.
- [7] W. Wu, X. Wang, X. Wang, S. Yang, X. Liu, Q. Chen, Mater. Lett. 63 (2009) 1788.
- [8] N. Yamanaka, M. Jiang, B. Key, C.P. Grey, J. Am. Chem. Soc. 131 (2009) 10525.
- [9] M. Nishijima, I.D. Gocheva, S. Okada, T. Doi, J.-I. Yamaki, T. Nishida, J. Power Sources 190 (2009) 558.
- [10] T. Li, L. Li, L. Cao, X.P. Ai, H.X. Yang, J. Phys. Chem. C 114 (2010) 3190.
- [11] R. Prakash, A. Mishra, A. Roth, C. Kubel, T. Scherer, M. Ghafari, M. Fichtner, J. Mater. Chem. 20 (2010) 1871.
- [12] R.F. Li, S.Q. Wu, Y. Yang, Z.Z. Zhu, J. Phys. Chem. C 114 (2010) 16813.
- [13] M. Zhou, L. Zhao, T. Doi, S. Okada, J.-I. Yamaki, J. Power Sources 195 (2010) 4592.
- [14] C. Li, L. Gu, S. Tsukimoto, P.A. van Aken, J. Maier, Adv. Mater. 22 (2010) 3650.
- [15] E. Gonzalo, A. Kuhn, F. Garcia-Alvarado, J. Power Sources 195 (2010) 4990.
- [16] N. Yabuuchi, M. Sugano, Y. Yamakawa, I. Nakai, K. Sakamoto, H. Muramatsu, S. Komaba, J. Mater. Chem. 21 (2011) 10035.
- [17] G.G. Amatucci, N. Pereira, F. Badway, M. Sina, F. Cosandey, M. Ruotolo, G. Cao, J. Fluorine Chem. 132 (2011) 1086.
- [18] A. Kitajou, H. Komatsu, K. Chihara, I. D. Gocheva, S. Okaga, J.-I. Yamaki, 198, 389 (2012).
- [19] S. Lerner, H.N. Seigler, J. Electrochem. Soc. 117 (1970) 574.
- [20] P.L. Crouse, J. Phys. Chem. Solids 50 (1989) 369.
- [21] T. Roisnel, J. Rodriguez-Carjaval, Fullprof Manual, Institut Laue-Langevin, Grenoble, 2002.
- [22] Joint Committee on Powder Diffraction Standards, File No. JCPDS Card, 85-0404.
- [23] D.G. Karraker, P.K. Smith, Inorg. Chem. 31 (1992) 1118.
- [24] R. De Pape, G. Ferry, Mat. Res. Bull. 12 (1986) 917.
- [25] R.D. Shannon, Acta Crystallogr. Sect. A Cryst. Phys. Diffraction. Theor. Gen. Crystallogr. 41 (1976) 653.
- [26] S.W. Oh, S.-T. Myung, S.-M. Oh, K.H. Oh, K. Amine, B. Scrosati, Y.-K. Sun, Adv. Mater. 22 (2010) 4842.
- [27] H.-G. Jung, S.-T. Myung, C.S. Yoon, S.-B. Son, K.H. Oh, K. Amine, B. Scrosati, Y.-K. Sun, Energy Environ. Sci. 4 (2011) 1345.
- [28] C.D. Wagner, W.M. Riggs, L.E. Davis, J.F. Moulder, Handbook of X-Ray Photoelectron Spectroscopy, Perkin Elmer Corp., Physics and Electronics Division, Eden Prairie, MN, 1979.
- [29] S.-T. Myung, K. Izumi, S. Komaba, Y.-K. Sun, H. Yashiro, N. Kumagai, Chem. Mater. 17 (2005) 3695.
- [30] S.-T. Myung, S. Komaba, N. Hirotsaki, K. Hosoya, N. Kumagai, J. Power Sources 143 (2005) 645.
- [31] S.-T. Myung, S. Komaba, K. Kurihara, K. Hosoya, N. Kumagai, Y.-K. Sun, I. Nakai, M. Yonemura, T. Kamiyama, Chem. Mater. 18 (2006) 1658.
- [32] S.W. Oh, S.-T. Myung, S.-M. Oh, C.S. Yoon, K. Amine, Electrochim. Acta 55 (2010) 1193.
- [33] S.-M. Oh, S.-T. Myung, J.B. Park, B. Scrosati, K. Amine, Y.-K. Sun, Angew. Chem. Int. Ed. 20 (2012) 1853.
- [34] F. Wang, R. Robert, N.A. Chernova, N. Pereira, F. Omenya, F. Badway, X. Hua, M. Ruotolo, R. Zhang, J. Wu, V. Volkov, D. Su, B. Key, M.S. Whittingham, C.P. Grey, G.G. Amatucci, Y. Zhu, J. Graetz, J. Am. Chem. Soc. 133 (2011) 18828.